photonics

MDPI

Article

Side-lobe Level Reduction of an Optical Phased Array Using Amplitude and Phase Modulation of Array Elements Based on Optically Injection-Locked Semiconductor Lasers

Anh Hang Nguyen, Jun-Hyung Cho, Ho-Jun Bae and Hyuk-Kee Sung *

School of Electronic and Electrical Engineering, Hongik University, Seoul 04066, Korea; hangna16@gmail.com (A.H.N.); kadokal@hotmail.com (J.-H.C.); hojun0616@naver.com (H.-J.B.)
* Correspondence: hksung@hongik.ac.kr; Tel.: +82-2-320-3037

Received: 21 January 2020; Accepted: 22 February 2020; Published: 24 February 2020



Abstract: The side-lobe level (SLL) in optical phased array (OPA) systems should be reduced to ensure their high performance. We investigate theoretically the performance of an OPA based on optically injection-locked (OIL) semiconductor lasers. The phase and amplitude of the OIL laser are modulated by controlling the injection-locking parameters to reduce the SLL as well as to achieve beam steering. We successfully achieved an SLL reduction of >16 dB when compared with the uniform amplitude profile based on the application of the Taylor window function profile to the injection-locked OPA elements. The reduced SLL and high power efficiency achieved in this study can expedite the use of OPA in real field applications, such as free-space communication, imaging, and light detection and ranging (LIDAR).

Keywords: optical injection locking; optical phased array; optical modulation; side-lobe level reduction

1. Introduction

Optical phased array (OPA) is a diffraction-based technology used to generate narrow optical beams that can be steered nonmechanically by modulating the amplitudes and phases of the OPA elements [1–3]. Owing to its advantages, including its light weight, small size, and nonmechanical beam steering, OPA technology has attracted considerable attention and has been adopted in numerous applications, such as free-space optical communications [4–6], light detection and ranging (LIDAR) [7], three-dimensional holography [8], and in biomedical imaging [9]. In the OPA configuration, the optical beam of each OPA element is fed by optical light sources, which are typically lasers. The optical sources are modulated by external optical components, such as amplitude/phase modulators [3,10,11]. In other OPA configurations, the laser arrays are frequency-locked to coherent optical signals by using either electro-optical phase locked loops or an optical injection-locking technique, whereby the optical signals are directly modulated to achieve phased-array optical signals without the use of an external modulator [3,12,13]. The latter OPA configurations have various advantages when compared with the former OPA configurations, including compactness, low loss, and low power consumption [12,13].

The key performance indicators of OPA systems include the steering angle, scanning speed, power consumption, efficiency, and the spatial beam quality, which is affected by unwanted side lobes [8,14,15]. The previously reported OPA technologies exhibit a steering angle of ~80°, beam widths as narrow as ~0.03°, and scanning speed of a few nanoseconds, which allow their ready use in real field applications. Among the performance indicators, the side-lobe level (SLL)—defined as the ratio of the side lobe power to the main lobe power of a far-field radiation pattern—is one of the

important performance indicators for the OPA used in real-field applications. The SLLs are reported to be relatively high, approximately equal to −12 dB [10–13]. The required SLL for practical applications is expected to be 30 dB to prevent unwanted effects, such as false target indications and interference signals [1,3]. Consequently, significant reduction of the SLL is fundamental to ensure high performance of OPA applications in high-fidelity areas, such as in the military, medicine, and communications [4–9].

Herein, we propose the application of a novel amplitude profile to the OPA elements by using the optical amplitude (AM) and phase modulation (PM) of optically injection-locked (OIL) semiconductor lasers to increase the SLL reduction as well as to achieve beam steering with increased frequency stability. The proposed OPA uses a master laser (ML) and a slave laser (SL) array to construct the OIL laser configurations. The SL array is frequency-locked to the single ML. The injection- locking parameters, detuning frequency, and injection ratio between the ML and each SL are changed to achieve the desired AM and PM.

We first introduce the concept of the active OPA configuration based on the OIL laser. We calculate the required profile of the amplitude and phase distributions of the optical elements to achieve an increased SLL reduction. The optical signal of each OPA element that enables the required amplitude and phase profile can be generated by controlling the injection-locking parameters between the ML and SL. The process is presented in detail by introducing the relationship between the injection-locking parameters and injection-locked amplitude/phase in the injection-locking map. Finally, we demonstrate a theoretical improvement of the OPA far-field pattern based on OIL laser arrays with the amplitude profile of a Taylor window function. The OIL-based OPA with the amplitude profile of a Taylor window function yielded a considerably low SLL value of 30 dB, which exhibited a reduction of >16 dB when compared with the uniform amplitude profile case. The optical beam profile of the OIL-based OPA maintained an enhanced reduction in the SLL performance during beam scanning. Consequently, the reduced SLL performance and high power efficiency achieved with the simple OPA configuration support the viewpoint that amplitude and phase modulation of OIL lasers can expedite the use of OPA in current real field applications, such as free-space communication, imaging, and LIDAR [4–9].

2. Active OPA Based on an OIL Laser

Figure 1a shows the schematic of the optical amplitude/phase modulation based on the OIL laser. The OIL laser configuration consists of two lasers, namely, the ML and SL. The optical signal of the ML with a field amplitude A_{ML}, frequency f_{ML}, and an optical phase, are injected to the SL. When the two injection-locking parameters, namely the detuning frequency ($\Delta f = f_{ML} - f_{free,SL}$) and injection ratio ($R = {A_{ML}}^2/{A_{free,SL}}^2 = S_{ML}/S_{free,SL}$), are properly controlled within the stable locking regime, the SL output yields the injection-locked output at the same frequency as the ML frequency f_{ML} with a locked phase ϕ_L and a field amplitude A_L, respectively [16,17]. The notations $f_{free,SL}$, $A_{free,SL}$, and $S_{free,SL}$ denote the frequency, field amplitude, and photon number of the free-running SL, respectively, while f_{ML} and S_{ML} are the frequency and photon number of the ML, respectively. Both the field amplitude A_L and phase ϕ_L of the injection-locked output signal are functions of the two injection-locking parameters. Therefore, they can be modulated concurrently by controlling the injection-locking parameters. One of the injection-locking parameters, the injection ratio R, can be changed using various methods. These include the use of injection power control based on the insertion of the optical amplifier or attenuator in front of the SL, the use of direct power control of the ML, and the use of direct power control of the SL. The other injection-locking parameter, the detuning frequency Δf, can be changed by varying the optical frequency of the ML f_{ML} or the free-running frequency of the SL $f_{free,SL}$. For example, the free-running lasing frequency of the SL can be tuned by controlling the SL temperature at a constant ML frequency, which changes the detuning frequency Δf. We reported previously that the two locking parameters can be simultaneously controlled by changing the bias current of the semiconductor SL because both the output power and lasing frequency of the free-running SL are functions of the bias current of the semiconductor SL [16–18]. The AM and PM can be achieved with a high optical output power based on the direct AM of the SL without the use of

external amplitude and phase modulators [18]. The AM/PM optical signal configuration based on the physics of the OIL semiconductor laser is presented in Figure 1a.

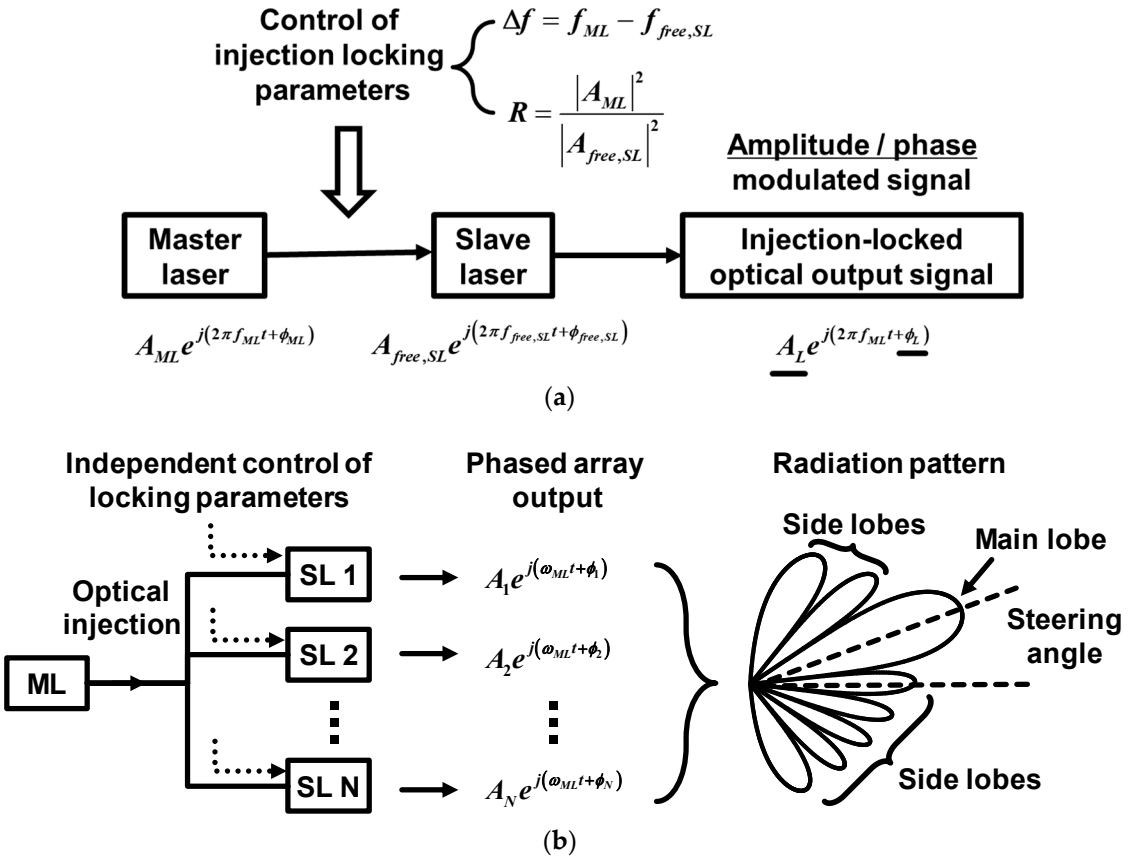


Figure 1. (**a**) Schematic of the optical amplitude/phase control based on the optically injection-locked (OIL) laser. (**b**) Schematic of the active optical phased array (OPA) based on OIL lasers. OIL-based OPA (ML: master laser, SL: slave laser).

Based on the advantages of the OIL semiconductor laser for OPA applications, such as its AM, PM, and the frequency-locking capabilities, we propose a novel active OPA, namely the OIL-based OPA, as shown in Figure 1b. The OIL-based active OPA is composed of a single ML and an array of amplitude-modulated SLs. The optical signal of the ML with field amplitude A_{ML}, frequency f_{ML}, and optical phase ϕ_L is injected into the SL arrays to produce frequency-locked optical signals at the ML frequency of f_{ML}. By changing the injection-locking conditions (e.g. applying the appropriate bias current to each SL element), the corresponding injection-locking parameters between the ML and each SL element can be controlled within a stable locking range. The amplitude A_L and phase ϕ_L of each OPA element can be controlled by the locking-parameters to produce the desired profiles of the phase and amplitude distributions of the OPA elements. Consequently, a narrow and steerable optical beam can be achieved by the spatially constructive interference of the AM/PM signals between the phased array elements. Figure 1b also shows the far-field pattern of the OIL–OPA, which consists of one main lobe and many side lobes. Owing to the high-power characteristic of the OPA elements along with strong injection-locking capability and direct modulation of the SL array, the proposed active OIL–OPA configuration exhibits high power efficiency as well as enhanced field pattern property owing to SLL reduction, as discussed in the following section.

3. Results

Figure 2 shows the schematic of the construction of the far-field radiation pattern of the OPA elements. The OPA structure consists of an array of N optical elements such that the optical signal of the n-th element is expressed as

$$\begin{aligned} E_{o,n} &= E_{i,n}\exp(-jk\ell_n) = A_n\exp[j\{\omega t+\phi_1-(n-1)\Delta\phi\}]\exp\{-jk(n-1)d\sin\theta\} \\ &= A_n\exp[j(\omega t+\phi_n-k\ell_n)] \end{aligned} \quad (1)$$

where $E_{i,n}$ is the optical field of the n_{th} element at the OPA position, k is the wave number, ℓ_n $(=(n-1)d\sin\theta)$ is the distance from the n_{th} array element to the observation point, A_n is the optical field amplitude of the n_{th} element, ω is the optical angular frequency, $\phi_n(=\phi_1-(n-1)\Delta\phi)$ is the optical phase of the n_{th} element, $\Delta\phi$ is the phase difference between two elements, d is the distance between two elements, and the steering angle θ is the angle between the observation direction and the perpendicular component of the OPA axis (i.e., the y-axis in Figure 2). The total field expression of the N-element OPA at a far (observation) position is obtained as

$$\begin{aligned} \widetilde{E}_t &= \sum_{n=1}^{N}\widetilde{E}_{o,n} \\ &= A_1e^{j(\omega t+\phi_1-k\ell_1)}+A_2e^{j(\omega t+(\phi_1-\Delta\phi)-k(\ell_1-d\sin\theta))}+A_3e^{j(\omega t+(\phi_1-2\Delta\phi)-k(\ell_1-2d\sin\theta))}+\ldots+A_Ne^{j(\omega t+(\phi_1-(N-1)\Delta\phi)-k(\ell_1-(N-1)d\sin\theta))} \\ &= e^{j(\omega t+\phi_1-k\ell_1)}\cdot(A_1+A_2e^{j(-\Delta\phi+kd\sin\theta)}+A_3e^{j2(-\Delta\phi+kd\sin\theta)}+\ldots+A_Ne^{j(N-1)(-\Delta\phi+kd\sin\theta)}) \\ &= e^{j(\omega t+\phi_1-k\ell_1)}\cdot(\text{ArrayFactor}) \end{aligned} \quad (2)$$

where the array factor (AF) is defined as

$$AF \triangleq A_1+A_2e^{j(-\Delta\phi+kd\sin\theta)}+A_3e^{j2(-\Delta\phi+kd\sin\theta)}+\ldots+A_Ne^{j(N-1)(-\Delta\phi+kd\sin\theta)} = \sum_{n=1}^{N}A_ne^{j(n-1)(kd\sin\theta-\Delta\phi)}. \quad (3)$$

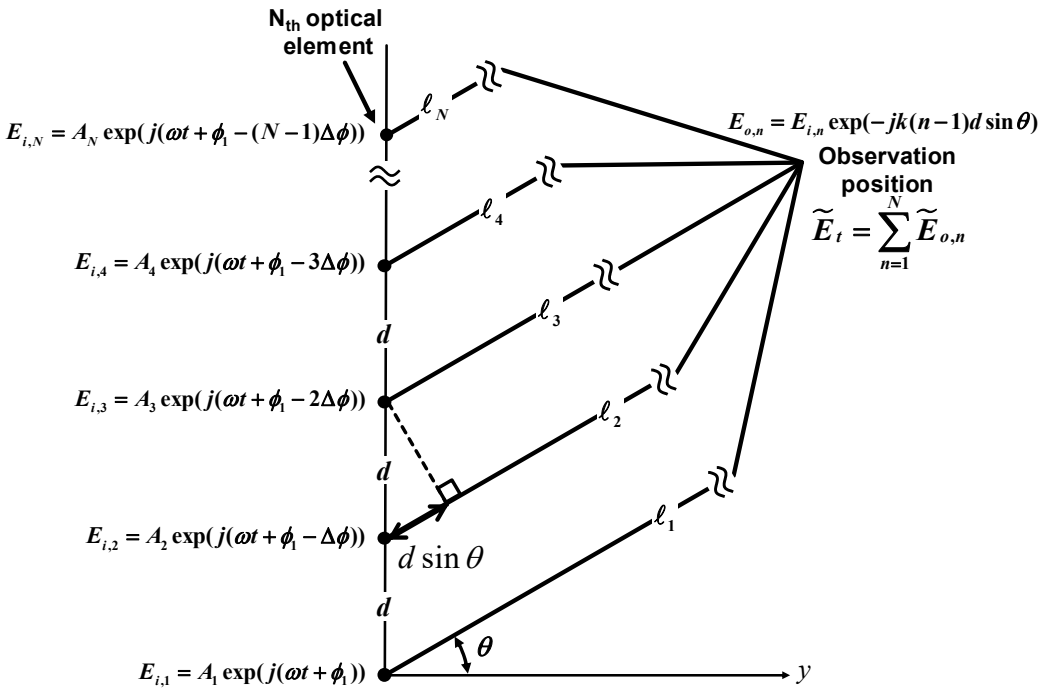


Figure 2. Construction of the far-field radiation pattern of the OPA elements.

Equation (2) shows that the far-field radiation pattern can be tailored by the AF. Equation (3) shows that the AF depends on the element field amplitude A_n, element number N, distance d, and phase difference $\Delta\phi$. This also shows that the element field amplitude A_n yields a finite Fourier

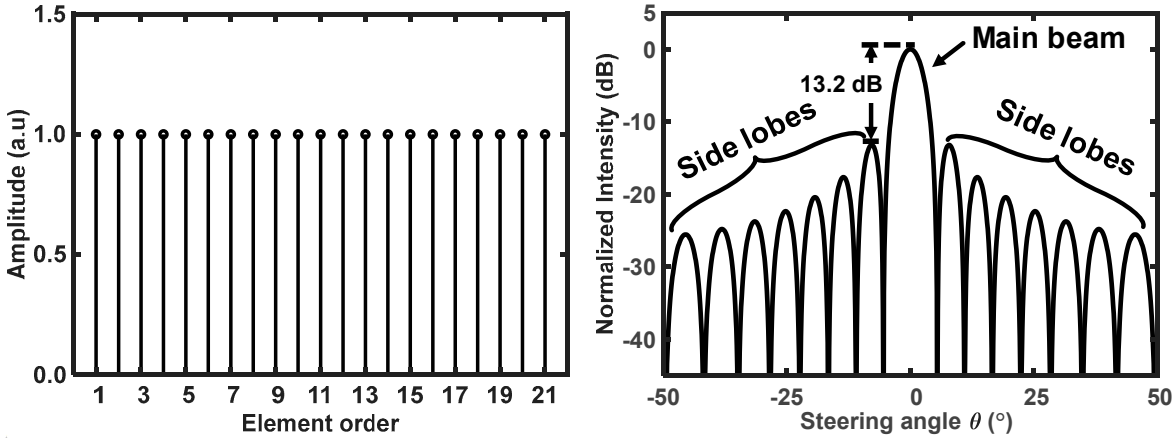
transform relation with the AF in which the element field amplitude A_n can be written in terms of a window-function in the form of [19],

$$A_n = \begin{cases} f(n), & 1 \le n \le N \\ 0, & otherwise \end{cases}. \tag{4}$$

Equation (3) shows that SLL, which is the one of the important performance indicators, exhibits a strong dependence on the distribution of the element field amplitude A_n. By choosing the appropriate window function $f(n)$ for the amplitude distribution A_n of the array elements, we can obtain the far-field radiation patterns with enhanced SLL performances. Figure 3a shows the distribution of the rectangular window functions of the 21 OPA elements in which all the relative amplitudes are equal. Figure 3b shows its Fourier transform (plotted based on a decibel scale), which is identical to the far-field radiation pattern of the OPA. The distance d between successive elements is set to be equal to half the optical wavelength, and the phase difference $\Delta\phi$ is set at 0°. Figure 3b shows the far-field radiation pattern of the OPA, which consists of a main lobe at the same angle as the maximum AF position as well as other side lobes. The steering angle θ_m of the main beam is

$$kd \sin\theta_m - \Delta\phi = 0, \text{then} \theta_m = \sin^{-1}\left(\frac{\Delta\phi}{kd}\right). \tag{5}$$

Equation (5) shows that the steering angle can be changed by controlling the phase difference between the OPA elements. Equation (5) shows that only one maximum value of the AF exists in the θ range of [−90°,90°] when the distance between two adjacent elements is not larger than half a wavelength. Figure 3b shows the high SLL of −13.2 dB, which limits the OPA performance.



(**a**) (**b**)

Figure 3. (**a**) Distribution of the rectangular window functions of 21 OPA elements. (**b**) Fourier transform (plotted on a decibel scale) of the rectangular window functions of the 21 OPA elements.

Herein, we introduce the Kaiser and Taylor windows [20,21], which can select specific SLL profiles to achieve the reduction of the SLL. Figure 4a shows the distribution of the element field amplitudes of the Kaiser and Taylor windows, the amplitude distributions of which are gradually tailed off to the edges. The Taylor window profile exhibits slightly increased amplitude profiles at the edges compared with the Kaiser window. Figure 4b shows the patterns of the Kaiser and Taylor windows. The target SLL is −30 dB. Both patterns exhibit significantly lower SLL than that of the rectangular window. The SLL adjacent to the main lobe in the case of the Kaiser window is slightly higher than that in the case of the Taylor window. Although the difference in the levels of the adjacent side lobes is small, the Taylor

window is a more appropriate selection for the field amplitude distribution A_n for the reduction of the SLL of the OPA pattern because the adjacent side lobes affect the OPA performance considerably.

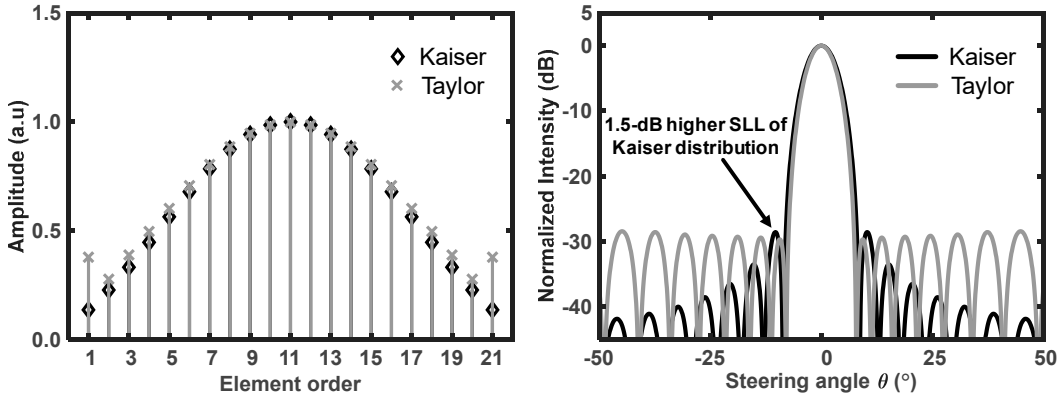


Figure 4. (**a**) Distributions of the Kaiser and Taylor window functions of 21 OPA elements. (**b**) Fourier transform (plotted on a decibel scale) of the Kaiser and Taylor window functions of the 21 OPA elements.

We propose the OPA configuration with the desired window function to achieve an improved SLL reduction performance. This is based on the AM/PM of the OIL semiconductor laser by controlling the injection-locking parameters. The PM in each SL element can produce the desired ϕ_n for beam steering, and the AM in each element can produce the desired field amplitude distribution A_n for the SLL reduction. Both the PM and AM processes can be simultaneously achieved in each SL by properly adjusting the injection-locking parameters. The relationship between the AM/PM amount and the injection-locking parameters is simulated based on the standard coupled-rate equations. The equations exhibit a dependence on the amplitude and phase of the OIL laser in the cases of the two injection-locking parameters, detuning frequency Δf and injection ratio R, as described in [16–18],

$$\frac{dS(t)}{dt} = \left\{g[N(t) - N_{tr}] - \gamma_p\right\}S(t) + 2\kappa\sqrt{S_{ML}S(t)}\cos[\phi(t) - \phi_{ML}], \tag{6}$$

$$\frac{d\phi(t)}{dt} = \frac{\alpha}{2}\left\{g[N(t) - N_{tr}] - \gamma_p\right\} - \kappa\sqrt{\frac{S_{ML}}{S(t)}}\sin[\phi(t) - \phi_{ML}] - \Delta\omega, \tag{7}$$

$$\frac{dN(t)}{dt} = J(t) - \gamma_n N(t) - g[N(t) - N_{tr}]S(t), \tag{8}$$

where $S(t)$, $\phi(t)$, and $N(t)$ are the photon number, phase, and carrier number of the injection-locked SL, respectively. Additionally, $\Delta\omega$ $(= 2\pi\Delta f)$ is the detuning angular frequency, g is the linear gain, N_{tr} is the transparency carrier number of the free running SL, γ_p is the photon decay rate, γ_n is the carrier decay rate, κ is the field coupling ratio between the ML and SL, and α is the linewidth enhancement factor of the laser. To achieve the desired amplitude A_L and phase ϕ_L, we directly controlled the bias current of the SL that is represented in Equation (8) by means of the number of electrons $J(t)$. The angular frequency difference between the ML and SLs $\Delta\omega$ also affects the phase of the injection-locked SLs, as described below [18].

$$\Delta\phi = \sin^{-1}\left\{-\frac{\Delta\omega}{\kappa\sqrt{1+\alpha^2}}\sqrt{\frac{S_L}{S_{ML}}}\right\} - \tan^{-1}\alpha, \tag{9}$$

and

$$S_L = \frac{S_{free,SL} - (\gamma_n/\gamma_p)\Delta N_0}{1 + (g\Delta N_0/\gamma_p)}, \tag{10}$$

where S_L and ΔN_0 are the steady-state photon and carrier numbers.

Therefore, the injection-locking equations listed above explain that the desired amplitudes and phases of the OPA elements can be achieved by varying the injection-locking parameters [16–18]. Figure 5 shows the injection-locking maps as a function of the detuning frequency and injection ratio. The stable locked regime in which the output signal is in steady state is depicted as a colored region. The injection-locking simulation parameters are listed in Table 1. The amplitude of the OIL laser as a function of the injection parameters of the SL is shown as a color scale map in Figure 5a. This map shows that the amplitude of the OIL laser can be modulated by controlling the two injection-locking parameters. Similarly, the color scale map in Figure 5b represents the phase shift of the injection-locked laser as a function of the injection-locking parameters. Any pair of the two injection-locking parameters, i.e., the injection ratio and detuning frequency, corresponds to specific positions on the map. Consequently, we can concurrently achieve the desired AM and PM of the SL by simultaneously controlling the relevant injection-locking parameters. It is noted that in real applications, the precise look-up tables for each OIL-OPA element, which reveal the relationship between the locking conditions and the amplitude/phase of the injection-locked SL, should be experimentally investigated.

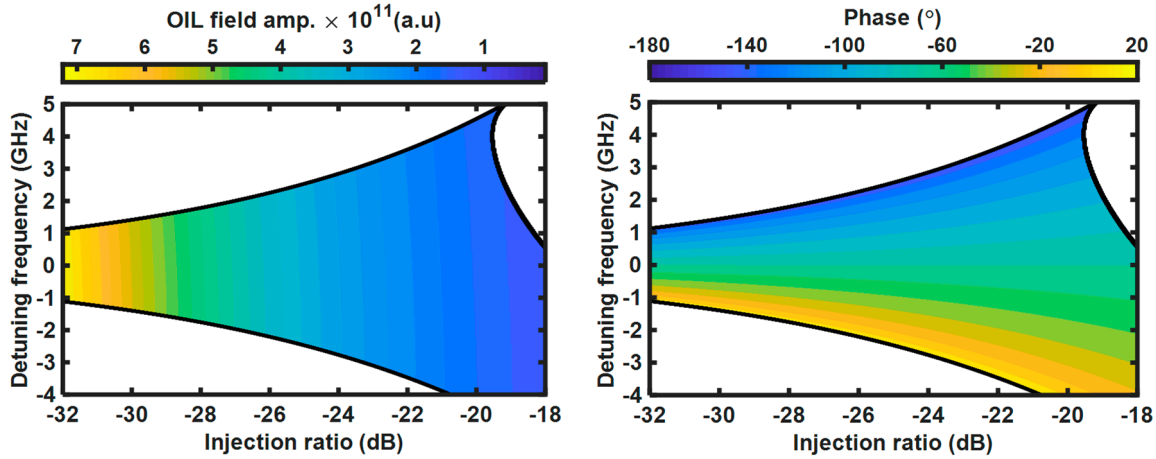


Figure 5. Injection-locking maps as a function of detuning frequency and injection ratio showing (**a**) amplitude modulation (AM) and (**b**) phase shift of the injection-locked laser.

Table 1. Simulation parameters.

Symbol	Quantity	Value	Unit
λ_0	Wavelength	1550	nm
g	Gain coefficient	1.1×10^{-12}	$m^3\ s^{-1}$
N_{tr}	Transparency carrier number	1.1×10^{24}	m^{-3}
γ_p	Photon decay rate	500	1/ns
γ_n	Carrier decay rate	0.5	1/ns
κ	Field coupling ratio	125	1/ns
α	Linewidth enhancement factor	2	

Figure 6 shows the distribution of the 21 elements of the OIL–OPA on the injection-locking map as a function of the detuning frequency and injection ratio. Each pair of the optical field amplitude and phase for an SL can be obtained by the corresponding pair of the detuning frequency and injection ratio, as shown in Figure 5. Therefore, by properly choosing the combination of the two injection-locking parameters, we can achieve the desired optical field amplitude distributions A_n and the desired phase distributions of $\phi_n (= \phi_1 - (n-1)\Delta\phi)$ for the 21 OPA elements. Figure 6 explains that the injection-locking parameters of the 21 elements of the OIL–OPA should be set at the cross-mark

positions to achieve the Taylor distribution of the amplitude distribution (as that shown in Figure 4a) and the target phase difference $\Delta\phi = +6°$ between the adjacent elements.

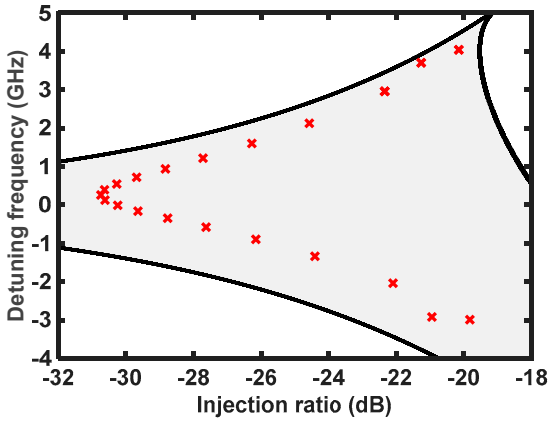


Figure 6. Distribution of 21 elements of an OIL–OPA on the injection-locking map as a function of the detuning frequency and injection ratio. This distribution achieved the Taylor AM distribution and a phase difference of $\Delta\phi = +6°$ between adjacent elements.

Figure 7a shows the far-field radiation pattern of the OPA without the control of the AM distribution (i.e., uniform distribution) for $\Delta\phi = +6°$ and the corresponding steering angle of $\theta = +1.9°$. It exhibits an SLL of −13.2 dB. Figure 7b shows the enhanced far-field radiation patterns of OPA based on the use of the Taylor window distribution according to the locking condition control of the OIL laser, as described in Figure 6. The calculation was performed for the beam angles of $+1.9°$ and $0°$. By achieving the appropriate injection-locking condition for each OPA element (as shown in Figure 6), we achieved OPA far-field radiation patterns with a low SLL of −30 dB, which corresponds to a reduction of >16 dB when compared with the uniform amplitude profile case for beam steering.

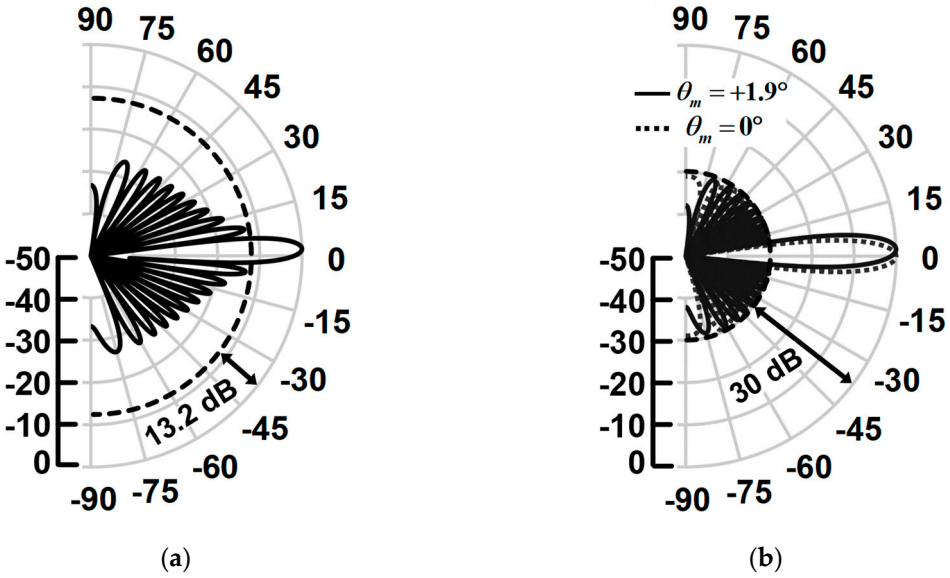


Figure 7. Far-field radiation patterns of 21-element OPA with (**a**) uniform amplitude distribution ($+1.9°$ direction), (**b**) Taylor window function profile ($+1.9°$ and $0°$ directions). θ_m is the steering angle.

The proposed OIL–OPA technique enables the high fidelity of the OPA beam patterns because of the reduced SLL as well as the other optical beam quality improvements, such as laser chirp reduction,

narrow beam performance, and relative intensity noise reduction, which are the inherent advantages of the OIL laser.

4. Conclusions

We proposed and numerically simulated the improvement of the SLL performance of OPA by AM and PM based on the OIL laser configuration. The two essential modulation processes of AM and PM were achieved simultaneously in the injection-locked SL based on the appropriate control of the laser locking condition. We calculated the relationship between the locking condition and AM/PM, and applied a desired Taylor window function on each OPA element. We achieved the reduction of the SLL and maintained the advantages of the OIL laser within a stable locking range. By controlling the injection-locking parameters and the application of the desired AM/PM for beam steering and SLL reduction, we achieved an SLL of −30 dB, which corresponds to a reduction of > 16 dB when compared with the uniform amplitude distribution of the OPA. The OIL–OPA configuration with high SLL reduction, high power efficiency, and frequency-locking capability indicates the tremendous application potential of the OPA in various fields, including free-space communications, LIDAR, and optical imaging.

Author Contributions: Conceptualization, H.-K.S., J.-H.C., H.-J.B., and A.H.N.; Methodology, H.-K.S., J.-H.C., and H.-J.B.; Investigation, A.H.N.; Formal Analysis, H.-K.S., J.-H.C., H.-J.B., and A.H.N.; Writing, H.-K.S., J.-H.C., and A.H.N. All authors have read and agreed to the published version of the manuscript.

Funding: This work was funded by the National Research Foundation of Korea (NRF) under the Basic Science Research Program (No. NRF-2019R1F1A1040959), and in part by the Korea Electric Power Corporation (No. R17XA05-74).

Conflicts of Interest: The authors declare no conflict of interest. The funding sponsors had no role in the design of the study; in the collection, analyses, or interpretation of data; in the writing of the manuscript, and in the decision to publish the results.

References

1. Balanis, C.A. Arrays: Linear, Planar, and Circular. In *Antenna Theory Analysis and Design*, 3rd ed.; John Wiley and sons: Hoboken, NJ, USA, 2005; pp. 283–384.
2. McManamon, P.F.; Dorschner, T.A.; Corkum, D.L.; Friedman, L.J.; Hobbs, D.S.; Holz, M.; Liberman, S.; Nguyen, H.Q.; Resler, D.P.; Sharp, R.C.; et al. Optical phased array technology. *Proc. IEEE* **1996**, *84*, 268–298. [CrossRef]
3. Heck, M. Highly integrated optical phased arrays: Photonic integrated circuits for optical beam shaping and beam steering. *Nanophotonics* **2016**, *6*, 93–107. [CrossRef]
4. Polishuk, A.; Shlomi, A. Communication performance analysis of microsatellites using an optical phased array antenna. *Opt. Eng.* **2003**, *42*, 2015–2024. [CrossRef]
5. Byrd, M.J.; Poulton, C.V.; Khandaker, M.; Timurdogan, E.; Vermeulen, D.; Watts, M.R. Free-space communication links with transmitting and receiving integrated optical phased arrays. *Proc. Frontiers Opt. Laser Sci.* **2018**, *FTu4E.1*, 1–2.
6. Rabinovich, W.S.; Goetz, P.G.; Pruessner, M.; Mahon, R.; Ferraro, M.S.; Park, D.; Fleet, E.; DePrenger, M.J. Free space optical communication link using a silicon photonic optical phased array. *Proc. SPIE* **2015**, *9354*, 1–6.
7. Poulton, C.V.; Yaacobi, A.; Cole, D.B.; Byrd, M.J.; Raval, M.; Vermeulen, D.; Watts, E.R. Coherent solid-state LIDAR with silicon photonic optical phased arrays. *Opt. Lett.* **2017**, *42*, 4091–4094. [CrossRef] [PubMed]
8. Zhou, J.; Sun, J.; Yaacobi, A.C.; Poulton, V.; Watts, M.R. Design of 3D Hologram Emitting Optical Phased Arrays. In Proceedings of the Advanced Photonics 2015, Massachusetts, MA, USA, 27 June–1 July 2015; pp. 1–3.
9. Fatemi, R.; Abiri, B.; Hajimiri, A. An 8 × 8 heterodyne lens-less OPA camera. In Proceedings of the Conference on Lasers and Electro-Optics 2017, San Jose, CA, USA, 14–19 May 2017; pp. 1–2.
10. Fatemi, R.; Khachaturian, A.; Hajimiri, A. A low power PWM optical phased array transmitter with 16° field-of-view and 0.8° beamwidth. In Proceedings of the 2018 IEEE Radio Frequency Integrated Circuits Symposium (RFIC), Philadelphia, PA, USA, 10–12 June 2018; pp. 28–31.

11. Acoleyen, K.V.; Rogier, H.; Baets, R. Two-dimensional optical phased array antenna on silicon-on-insulator. *Opt. Express* **2010**, *18*, 13655–13660. [CrossRef]
12. Sayyah, K.; Efimov, O.; Patterson, P.; Schaffner, J.; White, C.; Seurin, J.F.; Xu, G.; Miglo, A. Two-dimensional pseudo-random optical phased array based on tandem optical injection locking of vertical cavity surface emitting lasers. *Opt. Express* **2015**, *23*, 19405–19416. [CrossRef]
13. Aflatouni, F.; Hashemi, H. An electronically controlled semiconductor laser phased array. In Proceedings of the 2012 IEEE MTT-S International Microwave Symposium Digest (MTT), Montreal, QC, Canada, 17–22 June 2012; pp. 1–3.
14. Henniger, H.; Wilfert, O. An introduction to free-space optical communications. *Radioengineering* **2010**, *19*, 203–212.
15. Behroozpour, B.; Sandborn, P.A.M.; Wu, M.C.; Boser, B.E. Lidar system architectures and circuits. *IEEE Commun. Mag.* **2017**, *55*, 135–142. [CrossRef]
16. Lee, H.; Cho, J.H.; Sung, H.K. Enhancement of the phase-modulation range by using cascaded injection-locked semiconductor lasers. *J. Korean Phys. Soc.* **2016**, *68*, 756–761. [CrossRef]
17. Lee, H.; Cho, J.H.; Sung, H.K. Theoretical analysis of a method for extracting the phase of a phase-amplitude modulated signal generated by a direct-modulated optical injection-locked semiconductor laser. *Opt. Eng.* **2017**, *56*, 1–6. [CrossRef]
18. Cho, J.H.; Cho, C.H.; Sung, H.K. Theoretical performance evaluation of optical complex signals based on optically injection-locked semiconductor lasers. *IEEE J. Sel. Top. Quantum Electron.* **2019**, *25*, 1–9. [CrossRef]
19. Brandwood, D. Array Beamforming. In *Fourier Transforms in Radar and Signal Processing*, 2nd ed.; Artech House: Boston, MA, USA, 2003; pp. 161–187.
20. Poularikas, A.D. Window. In *The Handbook of Formulas and Tables for Signal Processing*, 1st ed.; CRC Press LLC: Boca Raton, FL, USA, 1999; pp. 131–148.
21. Patil, A.K. Design and performance analysis of filters using a proposed window function. *IJRSI* **2017**, *4*, 66–71.



© 2020 by the authors. Licensee MDPI, Basel, Switzerland. This article is an open access article distributed under the terms and conditions of the Creative Commons Attribution (CC BY) license (http://creativecommons.org/licenses/by/4.0/).